Genetic Regulation of Enoyl-CoA Hydratase Domain-Containing 3 in Adipose Tissue Determines Insulin Sensitivity in African Americans and Europeans

Neeraj K. Sharma,[1] Chia-Chi Chuang Key,[2] Mete Civelek,[3] Martin Wabitsch,[4] Mary E. Comeau,[5] Carl D. Langefeld,[5] John S. Parks,[2] and Swapan K. Das[1]

Diabetes 2019;68:1508–1522 | https://doi.org/10.2337/db18-1229

Insulin resistance (IR) is a harbinger of type 2 diabetes (T2D) and partly determined by genetic factors. However, genetically regulated mechanisms of IR remain poorly understood. Using gene expression, genotype, and insulin sensitivity data from the African American Genetics of Metabolism and Expression (AAGMEx) cohort, we performed transcript-wide correlation and expression quantitative trait loci (eQTL) analyses to identify IR-correlated *cis*-regulated transcripts (*cis*-eGenes) in adipose tissue. These IR-correlated *cis*-eGenes were tested in the European ancestry individuals in the Metabolic Syndrome in Men (METSIM) cohort for trans-ethnic replication. Comparison of Matsuda index–correlated transcripts in AAGMEx with the METSIM study identified significant correlation of 3,849 transcripts, with concordant direction of effect for 97.5% of the transcripts. *cis*-eQTL for 587 Matsuda index–correlated genes were identified in both cohorts. Enoyl-CoA hydratase domain-containing 3 (*ECHDC3*) was the top-ranked Matsuda index–correlated *cis*-eGene. Expression levels of *ECHDC3* were positively correlated with Matsuda index, and regulated by *cis*-eQTL, rs34844369 being the top *cis*-eSNP in AAGMEx. Silencing of *ECHDC3* in adipocytes significantly reduced insulin-stimulated glucose uptake and Akt Ser^{473} phosphorylation. RNA sequencing analysis identified 691 differentially expressed genes in *ECHDC3*-knockdown adipocytes, which were enriched in γ-linolenate biosynthesis, and known IR genes. Thus, our studies elucidated genetic regulatory mechanisms of IR and identified genes and pathways in adipose tissue that are mechanistically involved in IR.

The deterioration of systemic insulin responses related to glucose (and other metabolite) handling is referred to as insulin resistance (IR) (1). Reduced insulin sensitivity, or IR, promotes glucose intolerance and is a forerunner of type 2 diabetes (T2D) (1). Longitudinal studies in high-risk individuals suggest that IR occurs years before glucose intolerance or β-cell failure (2). Thus, reduced insulin sensitivity is an intermediate phenotype and early marker of T2D risk. Diet, lifestyle, and other environmental factors play important roles in the etiology of IR. However, several lines of evidence, including differences in the prevalence of IR among ethnic groups, suggest that genetic factors are important influences on IR (3). Deciphering the underlying molecular defects and genetic regulatory mechanisms of insulin sensitivity is an unmet need to develop novel and safe therapeutic options to prevent IR and slow or halt progression to T2D and its devastating complications.

Previous efforts to understand the role of genetic factors in determining IR were primarily focused on identifying susceptibility loci (e.g., single nucleotide polymorphisms [SNPs]) by genetic association studies in human populations. Large-scale genetic association studies provide valuable insights into the genetic architecture of phenotypes such as fasting glucose and insulin (4–7); IR, whether derived from oral glucose tolerance tests (OGTTs), frequently sampled intravenous glucose tolerance tests, or euglycemic clamp studies (8–10); and T2D.

[1]Section of Endocrinology and Metabolism, Department of Internal Medicine, Wake Forest School of Medicine, Winston-Salem, NC
[2]Section of Molecular Medicine, Department of Internal Medicine, Wake Forest School of Medicine, Winston-Salem, NC
[3]Center for Public Health Genomics, Department of Biomedical Engineering, University of Virginia, Charlottesville, VA
[4]Division of Pediatric Endocrinology and Diabetes, Department of Pediatrics and Adolescent Medicine, University Medical Center Ulm, Ulm, Germany
[5]Division of Public Health Sciences, Department of Biostatistics and Data Science, Wake Forest School of Medicine, Winston-Salem, NC

Corresponding author: Swapan K. Das, sdas@wakehealth.edu

Received 20 November 2018 and accepted 3 April 2019

This article contains Supplementary Data online at http://diabetes.diabetesjournals.org/lookup/suppl/doi:10.2337/db18-1229/-/DC1.

Functional interpretation of those association signals remains challenging, and recent efforts were only nominally successful in defining genes specifically modulated by these SNPs (11,12). Alternative strategies are required for a more precise understanding of genetic regulatory mechanisms of IR.

Adipose tissue integrates various physiologic pathways, including glucose and fatty acid homeostasis (13). The failure of adipocytes to sequester excess fuel during nutritional abundance results in ectopic fat accumulation and is proposed as a trigger for systemic IR (1,14,15). Transcriptomic analyses by us and others suggest that IR results from a derangement in gene expression in tissues involved in glucose homeostasis, including adipose tissue (16–18). Interactions among genetic factors and dietary components likely determine variability in adipose tissue remodeling and expansion by modulating gene expression, leading to adipose tissue dysfunction and onset of IR. Genetic variants such as SNPs may determine tissue gene transcript levels. Thus, to identify genetic IR regulatory mechanisms, we focused on adipose tissue IR–correlated transcripts modulated by expression regulatory loci (expression quantitative trait loci [eQTL]). We hypothesized that expression of a substantial subset of IR-correlated genes, in part, is genetically driven and causally linked to altered insulin sensitivity. Further, we hypothesized that focused interrogation of these genes would help to identify novel susceptibility loci within a functional context.

Similar to most complex diseases, IR is a heterogeneous mix of molecular phenotypes caused by perturbations of multiple genes contributing to altered insulin sensitivity. To identify genetic IR regulatory mechanisms that are common in both African and European ancestry populations, we implemented a systems biological approach. Using gene expression, genotype, and insulin sensitivity data from an African American cohort, we identified insulin sensitivity–correlated *cis*-regulated transcripts (*cis*-eGenes) in adipose tissue. Data from a European ancestry cohort replicated 587 insulin sensitivity–correlated *cis*-eGenes. These analyses suggested that genetically regulated expression of adipose tissue enoyl-CoA hydratase domain-containing 3 (*ECHDC3*) may play an important role in determining insulin sensitivity. In vitro genetic silencing studies in a human adipocyte model were successful in elucidating cellular and molecular mechanisms for the role of *ECHDC3* in IR.

RESEARCH DESIGN AND METHODS

Human Subjects

Glucometabolic phenotype, gene expression, and genotype data available from 256 unrelated and individuals without diabetes in the African American Genetics of Metabolism and Expression (AAGMEx) cohort (18,19) were used to identify genetically regulated adipose tissue insulin sensitivity–correlated transcripts. Cohort participants were healthy, self-reported African American men and women residing in North Carolina, aged 18–60 years, with a BMI between 18 and 42 kg/m^2. All participants provided written informed consent under protocols approved by the institutional review boards at Wake Forest School of Medicine. A standard 75-g OGTT was used to evaluate insulin sensitivity and exclude individuals with diabetes. Fasting blood samples were drawn for DNA isolation and biochemical analyses. Subcutaneous adipose tissue biopsies were collected by Bergstrom needle from participants after an overnight fast. Clinical, anthropometric, and physiological characteristics of the AAGMEx cohort have previously been described (18).

We sought to replicate our findings in AAGMEx cohort using adipose tissue gene expression and genotype data from the European Ancestry individuals in Metabolic Syndrome in Men (METSIM) cohort (Finland [N = 770]) (20). In AAGMEx, insulin sensitivity was measured by both OGTT and frequently sampled intravenous glucose tolerance tests. However, the Matsuda index, a measure of insulin sensitivity derived from OGTT, was available for both the AAGMEx and METSIM cohorts and was used in this study as the primary phenotype. Laboratory, statistical, and bioinformatic methods are described briefly below.

Laboratory Measures and Physiologic Phenotypes

Details of clinical laboratory measures have previously been described (18,20). In brief, for the AAGMEx cohort, plasma glucose levels were analyzed at a Clinical Laboratory Improvement Amendments–certified commercial laboratory (LabCorp). Plasma insulin was measured using an immunochemiluminometric assay (Invitron Limited, Monmouth, U.K.). Plasma glucose and insulin data from five OGTT time points (0, 30, 60, 90, and 120 min) were used to calculate the Matsuda insulin sensitivity index (http://mmatsuda.diabetes-smc.jp/MIndex.html). Insulin sensitivity in the METSIM cohort was evaluated by calculating Matsuda index from three OGTT data points (0, 30, and 120 min).

Gene Expression Analyses and Genotyping Methods

Details of adipose tissue gene expression analyses, genotyping, and data quality-control methods for both cohorts have previously been published (18–20). Genome-wide expression data in AAGMEx were generated using HumanHT-12 v4 Expression BeadChip (Illumina, San Diego, CA) whole-genome gene expression arrays. Data were submitted to the Gene Expression Omnibus (GEO) (identification no. GSE95674). In the METSIM cohort, subcutaneous adipose tissue expression data were generated by Affymetrix U219 arrays and submitted to GEO (identification no. GSE70353). Infinium HumanOmni5Exome-4 v1.1 DNA Analysis BeadChips (Illumina) were used to genotype DNA samples from the AAGMEx cohort based on the manufacturer's instructions. METSIM samples were genotyped using the Illumina HumanOmniExpress BeadChip array and the Illumina HumanCoreExome array.

Bioinformatics and Statistical Analyses

As described previously (18), in the AAGMEx data set, genome-wide gene expression data (probe level) were extracted using Illumina GenomeStudio V2011.1. Expression levels were $\log_2$ transformed, robust multiarray average normalized (includes quantile normalization), and batch corrected using ComBat (https://www.bu.edu/jlab/wp-assets/ComBat/). Details of the gene expression data processing for METSIM have previously been published (20).

In AAGMEx, genotype data were examined to verify sample and SNP quality. Genotype assays of 4,210,443 SNPs passed technical quality filters. Genotypes from 2,296,925 autosomal SNP assays (representing 2,210,735 unique high-quality genotyped SNPs with minor allele frequency [MAF] >0.01 and Hardy-Weinberg equilibrium P value $>1 \times 10^{-6}$) were used in our initial eQTL analyses (19). We imputed these genotyped SNPs to the 1000 Genomes data set (1KGP, phase 3 cosmopolitan reference panel) using the genotype imputation program Minimac3, implemented on the Michigan Imputation Server (https://imputationserver.sph.umich.edu/). The combined set of 14,502,313 autosomal genotyped and imputed SNPs was used for expanded eQTL analyses for selected Matsuda index–correlated transcripts. After quality control and genotype imputation of the 681,789 directly genotyped variants, the METSIM study used 7,677,146 variants (MAF $\geq$0.01) for eQTL analysis (20).

To test for associations between insulin sensitivity and expression level in the AAGMEx cohort, we computed a linear regression model using R(glm) software with the Matsuda index (natural log transformed) as the outcome and expression level ($\log_2$) as the predictor. Models included age, sex, and African ancestry proportion (admixture estimates were computed using the ADMIXTURE program [http://software.genetics.ucla.edu/admixture/index.html]) as covariates (Supplementary Fig. 1). A secondary analysis included BMI as an additional covariate. We computed P values adjusted for Benjamini-Hochberg false discovery rate (FDR) (q value). Expression of a transcript probe correlated with Matsuda index at $q < 0.01$ was considered significant, excluding probes with a SNP within the probe sequence. We also correlated the Matsuda index with each transcript using Spearman semipartial correlation coefficients adjusted for age, sex, and ancestry proportion (admixture). We used the DAVID functional annotation tool (v6.9) (https://david.ncifcrf.gov/) and Ingenuity Pathway Analysis (IPA) (Build version: 470319M, Content version: 43605602) (https://apps.ingenuity.com/) to identify enrichment of Matsuda index–correlated genes in biological pathways. In the METSIM data set, regression analyses were computed to evaluate correlations between adipose tissue gene expression and cardiometabolic-related traits, including the Matsuda index (20). We compared results from the METSIM and AAGMEx cohorts. Expression of a transcript correlated with Matsuda index at $q < 0.05$ in both cohorts and showing the same direction of effect was considered statistically replicated.

We also conducted *cis*-eQTL analyses (i.e., within $\pm$ 500 Kb 5′ and 3′ of respective transcript). For each transcript probe, we computed linear regression with the $\log_2$-transformed expression value as the outcome and an additive genetic model for the SNP as implemented in the *R* package MatrixEQTL, with age, sex, and African ancestry proportion as covariates in AAGMEx. *Cis*-eQTL with $P < 2.96 \times 10^{-5}$ corresponding to a q value <0.01 (or <1.0%) were considered significant (19). A secondary eQTL analysis included BMI as an additional covariate. Results from factored spectrally transformed linear mixed model (FaST-LMM) eQTL analysis in the METSIM cohort (https://systems.genetics.ucla.edu/) were used for comparison (20). Considering the difference in sample sizes for eQTL analyses, transcripts with *cis*-eQTL P value $< 2.46 \times 10^{-4}$ in METSIM (corresponding to 1% FDR) (20) and $P \leq 1.75 \times 10^{-4}$ (corresponding to $q < 0.04$) in AAGMEx were considered statistically replicated *cis*-eGenes.

To test for an association between a SNP and Matsuda index (natural log transformed) in AAGMEx, a linear regression model (SNPLASH) (https://www.phs.wakehealth.edu/public/home.cfm) was computed that included age, sex, and African ancestry proportion as covariates. The primary inference was based on the additive genetic model. Similar linear regression model analysis adjusting for age was implemented in R to test association between *cis*-expression regulatory single nucleotide polymorphisms (*cis*-eSNPs) in selected loci and Matsuda index in METSIM.

Studies in Cultured Adipocyte Models

Gene expression analysis in adipose tissue from human cohorts identified enoyl-CoA hydratase domain-containing 3 (*ECHDC3*) as the top-ranked Matsuda index–correlated *cis*-eGene (see RESULTS). Thus, we studied the expression of *ECHDC3* at different stages of differentiation in human adipose stroma-derived stem cells (hADSCs). The hADSCs (AG17928 and AG172929) derived from abdominal subcutaneous tissue samples donated by two different women were obtained from Coriell Cell Repositories (Camden, NJ). To identify the role of *ECHDC3* in adipocytes by knocking down its expression, we used Simpson-Golabi-Behmel syndrome (SGBS) preadipocytes, a well-characterized human adipocyte cell model (21) that is more amenable to genetic manipulation than hADSCs and has an expression profile after differentiation that closely mimics mature adipocytes. We grew hADSC and SGBS cells under standard culture condition in DMEM/Ham's F-12 (1:1 v/v) adipocyte basal medium (BM-1; ZenBio, Inc.; Research Triangle Park, NC) supplemented with 10% FBS and antibiotics. Cells were differentiated to adipocytes using adipocyte differentiation medium (DM2; ZenBio) for 7 days and maintained for an additional 7 days in adipocyte maintenance medium (AM-1; ZenBio) for complete maturation of adipocytes following the vendor-recommended protocol.

For stable RNA interference, the *ECHDC3* gene was silenced by infecting the SGBS preadipocytes with lentiviral particles to deliver gene-specific shRNA expression

vectors (sc-90758-V; Santa Cruz Biotechnology, Santa Cruz, CA) (a pool of transduction-ready viral particles containing three target-specific constructs that encode shRNA) in the presence of polybrene (sc-134220 [8 μg/mL]; Santa Cruz Biotechnology) according to the manufacturer's protocol. A control shRNA, lentiviral Particles-A (sc-108080; Santa Cruz Biotechnology) (encodes a scrambled shRNA sequence that will not lead to the specific degradation of any known cellular mRNA), was used as a negative control. Cells successfully transduced and stably expressing shRNA were selected using 2 μg/mL puromycin (A1113803; Gibco, Thermo Fisher Scientific).

Total RNA was isolated using an RNAeasy kit (Qiagen) from three sets of cells: *1*) undifferentiated hADSC and SGBS cells, *2*) hADSC and SGBS cells at different stages of differentiation, and *3*) *ECHDC3* shRNA and control shRNA–expressing SGBS cells at the 14th day of differentiation. RNA samples were reverse transcribed using a QuantiTect reverse transcription kit (Qiagen) based on the manufacturer's protocol. For determination of expression levels at different stages of adipocyte differentiation and for confirmation of shRNA-mediated downregulation, *ECHDC3* expression was measured in cDNA by quantitative real-time PCR (qRT-PCR) using Power SYBR green chemistry (Applied Biosystems, Inc., Foster City, CA). Oligonucleotide primers used to amplify *ECHDC3* were 5′-ACGGCATAAGGAACATCGTC-3′ (forward) and 5′-AAAACACAGGCCCCTCAG-3′ (reverse). The expression of target genes was normalized to the expression of an endogenous control gene, 36B4/RPLP0. Two independent experiments with three biological replicates for each treatment condition were performed for confirmation of successful *ECHDC3* knockdown by gene-specific shRNA.

Glucose Uptake Assay

Similar to a published study (22), on day 14 of differentiation, the control shRNA and *ECHDC3* shRNA (ECHDC3-KD) SGBS cells grown in biological triplicates in sixwell plates were washed with Dulbecco's PBS and preincubated with HEPES-buffered Krebs-Ringer solution (Alfa Aesar J67795) for 6 h at 37°C. After preincubation, the cells were incubated with or without 1 μmol/L insulin in Krebs-Ringer solution for 20 min. Next, 0.5 μCi/mL labeled 2-deoxy-D-[^{3}H]glucose and 0.25 mmol/L D-glucose were added for an additional 20 min at 37°C. Reactions were terminated by placing the cells onto the ice and washing three times with ice-cold Dulbecco's PBS. The cells were solubilized with 1 mL of 0.2 N NaOH per well and incubated overnight at room temperature with constant shaking. Radioactivity and protein content in cell lysates were measured using liquid scintillation spectroscopy and bicinchoninic acid assays, respectively. Cellular radiolabeled glucose uptake was normalized to cell protein content.

Western Blots to Determine Insulin-Stimulated Akt Phosphorylation

On the 14th day of differentiation, control shRNA and *ECHDC3* shRNA (ECHDC3-KD) SGBS cells (in sixwell plates) were washed once with 0.1% BSA-PBS and serum starved in 0.1% BSA-PBS for 30 min. Cells were then stimulated with or without 100 nmol/L insulin for 15 min (23). Cells were harvested using 200 μL RIPA buffer (no SDS) per well of a sixwell plate. Cell lysates were sonicated (3 pulses for 3 s) on ice and centrifuged (12,000 rcf for 15 min), and protein concentrations in clear lysates were measured by bicinchoninic acid assays. Molecular weight markers and heat-denatured cell lysates containing 10 μg protein were loaded in each well for electrophoretic separation on a 10% SDS-PAGE gel (30 min at 80 V and 90 min at 110 V). Protein bands were transferred to polyvinylidene difluoride membranes (3.5–4 h at 65 V or 400 mA). Membranes were blocked with 5% nonfat milk and 0.1% Tween 20 in Tris-buffered saline (0.1% TBST) for 1 h at room temperature. Membranes were washed three times (5 min each) in 0.1% TBST. Blocked and washed membranes were then incubated overnight at 4°C in 0.1% TBST buffer containing 5% fatty acid–free BSA and primary phosphorylated Akt (pAkt) at Ser^{473} (1:1,000, cat. no. 4060; Cell Signaling Technologies), total Akt (1:1,000, cat. no. 4691; Cell Signaling Technologies), or GAPDH (1:2,000, cat. no. sc-32233; Santa Cruz Biotechnology) antibody. Membranes were then washed three times in 0.1% TBST (5 min each) and incubated with conjugated secondary antibody (1:5,000, cat. no. A9169, goat anti-rabbit IgG–horseradish peroxidase, Sigma-Aldrich, and cat no. sc-2031, goat anti-mouse IgG–horseradish peroxidase, Santa Cruz Biotechnology) in 0.1% TBST buffer containing 5% nonfat milk at room temperature for 1–2 h. Finally, membranes were washed (three washes of 0.1% TBST for 5 min each) and images were acquired using darkroom development techniques or cold camera for chemiluminescence.

RNA Sequencing and Bioinformatic Analyses

We performed genome-wide expression profiling of control and *ECHDC3* shRNA SGBS cells in triplicate at day 14 of differentiation by RNA sequencing (RNA-seq). RNA-seq experiments were performed at Beijing Genome Institute (BGI, Shenzhen, China). In brief, high-quality total RNA samples (RNA integrity number [RIN] $>$ 9.0) isolated from SGBS cells were treated with DNase I to remove DNA contamination, and then the mRNA was enriched by using oligo (dT) magnetic beads. Sequencing adaptor-ligated cDNA libraries were prepared from mRNA templates and were used with BGISEQ-500 RNA-seq technology to obtain $>$20 million single-end 50 base pair (bp) reads per sample. On average, 24,135,731 raw sequencing reads were generated per sample, and after filtering low-quality reads, on average 23,841,269 clean reads were obtained. Clean reads were mapped to the human reference genome using the HISAT/Bowtie2 tool (24,25). The average mapping ratio

with the reference gene was 84.41% and average genome mapping ratio was 96.51%. Gene expression levels were quantified as fragments per kilobase million (FPKM) values using RSEM software (26). Differentially expressed genes (DEGs) between groups were screened using NOISeq (27). DEGs with Bayes posterior probability >70% in NOISeq and average $\log_2$ fold change ± 0.58 were considered significant. IPA (https://apps.ingenuity.com/) (Build version: 481437M, Content version: 39480507) was used to identify enrichment of DEGs in biological pathways.

RESULTS

Expression of Subcutaneous Adipose Tissue Transcripts Enriched for Salient Biological Pathways Is Correlated With Matsuda Index of Insulin Sensitivity in African Americans

Individuals in the AAGMEx cohort had a broad range of insulin sensitivity as measured by OGTT-derived Matsuda index (mean ± SD 6.2 ± 6.7). High-quality adipose tissue gene expression and Matsuda index data (N = 246 subjects) were used to determine correlations between insulin sensitivity and adipose tissue transcript expression levels. Expression of 5,102 transcripts (probes representing 4,273 Entrez Gene IDs) in adipose tissue was significantly correlated (q value <0.01) with Matsuda index (Supplementary Table 1). Matsuda index was positively and negatively correlated, respectively, with the expression of 2,645 and 2,457 adipose transcripts. Among these transcripts, 83% (4,239 probes) remain significantly associated ($P < 0.05$) with Matsuda index even after additional adjustment for BMI. Membrane-spanning 4-domains subfamily-A member 6A (*MS4A6A*) was the most significant negatively (inversely) correlated transcript (ILMN_1721035, $\beta = -1.06$, $P = 4.27 \times 10^{-24}$), whereas zinc-binding α-2-glycoprotein 1 (*AZGP1*) was the most significant positively correlated transcript (ILMN_1797154, $\beta = 1.33$, $P = 2.96 \times 10^{-23}$) with the Matsuda index (Table 1). Multiple probes putatively representing isoforms of 707 Entrez ID genes were correlated with the Matsuda index, including probes for 691 Entrez ID genes (e.g., three probes for *MS4A6A*) showing the same effect direction. However, probes for 16 Entrez ID genes (e.g., two probes for clusterin [*CLU*]) showed discordant directions of effect, suggesting isoform-specific roles of these genes in insulin sensitivity.

We found significant enrichment (Benjamini-Hochberg–corrected $P < 0.05$) of 205 canonical pathways (in IPA knowledgebase) among these Matsuda index–correlated transcripts in adipose tissue (Supplementary Table 2*A*). Gene expression profiles also suggested significant activation (activation z score >2) or repression ($z < -2$) of 41 pathways enriched in adipose tissue of insulin-sensitive individuals. Among the enriched pathways, expression profile of genes in oxidative phosphorylation (Benjamini-Hochberg–corrected $P = 1.58 \times 10^{-12}$, $z = 7.216$), EIF2 signaling ($P = 6.17 \times 10^{-8}$, $z = 3.111$), and valine degradation ($P = 7.24 \times 10^{-7}$, $z = 3.357$) pathways suggested significant activation, whereas genes in integrin signaling ($P = 4.47 \times 10^{-9}$, $z = -3.801$), IL-8 signaling ($P = 1.70 \times 10^{-6}$, $z = -3.204$), and Fcγ receptor–mediated phagocytosis in macrophage and monocyte ($P = 2.88 \times 10^{-6}$, $z = -3.904$) pathways suggested significant repression in insulin-sensitive individuals. Expression levels of 55 genes in oxidative phosphorylation pathways were positively, and of 33 genes in Fcγ receptor–mediated phagocytosis in macrophage and monocyte pathway were inversely, correlated with Matsuda index. DAVID functional annotation analysis using KEGG and GO annotation also validated the enrichment of multiple pathways (Supplementary Table 2*B*).

Correlation of Adipose Tissue Transcript Levels With Matsuda Index in African Americans Replicates in an Independent European Ancestry Cohort

Using adipose tissue expression data from METSIM and European ancestry cohorts, we sought replication of Matsuda index–correlated transcripts identified in African Africans. Individuals in the METSIM cohort also had a broad range of Matsuda index values (mean ± SD 7.3 ± 4.3). We compared the most significant Matsuda index–correlated probe for each gene in METSIM with transcripts significantly correlated with Matsuda index and matched for gene symbol annotation in AAGMEx. A total of 3,849 transcripts were significantly correlated ($q < 0.05$) with Matsuda index in both cohorts (Supplementary Table 3). Matsuda index was positively and inversely correlated with the expression of 2,047 and 1,708 adipose transcripts in both cohorts, respectively. (Supplementary Fig. 2*A*). Thus, our results suggest a strong replication of correlation and direction of effect for 97.5% of Matsuda index–correlated adipose tissue transcripts in independent cohorts of African and European ancestry individuals.

Matsuda Index–Correlated Transcripts Are Regulated by eQTL in African and European Ancestry Individuals

Our analyses in these cohorts suggested deranged expression of thousands of adipose tissue genes in those with IR. However, it is difficult to differentiate causal effects from reactive effects based on transcriptomic data. Genotype variations, including SNPs in regulatory regions of the genome or eQTL, may determine tissue transcript levels. The eQTL analyses integrate SNP genotypes with transcript expression profiles and provide evidence for genotype-dependent variations in transcript abundance. eQTL analyses identified significant *cis*-eSNPs for 587 Matsuda index–correlated transcripts in adipose tissue of AAGMEx and METSIM participants (FDR 4% and FDR 1%, respectively) (Supplementary Table 4). Top *cis*-eSNPs in one cohort showed high concordance in effect direction and strong correlation of effect sizes in the other cohort (Supplementary Table 4*A* and *B* and Supplementary Fig. 3). In the AAGMEx cohort, we also compared the eQTL analysis with and without adjustment for BMI. Of the 587 Matsuda index–correlated *cis*-eGenes that we report, 474 are

Table 1—Twenty most significantly correlated expression levels of subcutaneous adipose tissue transcripts with Matsuda insulin sensitivity index in AAGMEx

Probe ID	Symbol	Entrez Gene ID	β	SE of β	Adjusted R^2	*P* value	*q* value
ILMN_1721035	*MS4A6A*	64231	−1.06	0.093	0.365	4.27E-24	2.02E-19
ILMN_2397721	*GLB1*	2720	−1.94	0.174	0.361	1.01E-23	2.39E-19
ILMN_1796409	*C1QB*	713	−0.94	0.087	0.342	3.44E-22	2.71E-18
ILMN_1722622	*CD163*	9332	−1.01	0.095	0.338	6.67E-22	4.51E-18
ILMN_1805992	*KIAA1598*	57698	−1.51	0.144	0.333	1.91E-21	1.13E-17
ILMN_1745963	*FOLR2*	2350	−1.50	0.145	0.326	6.27E-21	2.97E-17
ILMN_1792473	*AIF1*	199	−1.19	0.117	0.319	2.16E-20	7.86E-17
ILMN_1740015	*CD14*	929	−1.20	0.118	0.317	2.97E-20	9.06E-17
ILMN_1757387	*UCHL1*	7345	−0.66	0.066	0.315	4.36E-20	1.15E-16
ILMN_1780533	*RNASE6*	6039	−2.42	0.241	0.314	5.50E-20	1.30E-16
ILMN_1740024	*NAALAD2*	10003	1.06	0.111	0.296	1.18E-18	1.22E-15
ILMN_1757882	*PPP1R16A*	84988	1.51	0.157	0.296	1.20E-18	1.22E-15
ILMN_3285959	*LOC645515*	645515	2.54	0.265	0.296	1.22E-18	1.22E-15
ILMN_1785284	*ALDH6A1*	4329	1.22	0.124	0.305	2.79E-19	4.41E-16
ILMN_1778104	*ACADM*	34	1.44	0.144	0.311	9.30E-20	2.00E-16
ILMN_1694106	*GPD1L*	23171	1.37	0.136	0.317	3.06E-20	9.06E-17
ILMN_1718924	*ETFA*	2108	1.76	0.175	0.317	3.02E-20	9.06E-17
ILMN_1690040	*TM7SF2*	7108	1.14	0.112	0.320	1.75E-20	6.89E-17
ILMN_1678323	*AASS*	10157	2.84	0.279	0.322	1.42E-20	6.12E-17
ILMN_1797154	*AZGP1*	563	1.33	0.120	0.355	2.96E-23	4.64E-19

Top 10 positively and top 10 inversely correlated genes are shown. Results for all significant probes are shown in Supplementary Table 1. β, β-coefficient value; *P* value, significance level of correlation of transcript level with Matsuda index; adjusted R^2, proportion of the variation in Matsuda index (outcome) explained by expression levels (predictor) in linear regression analysis adjusted for age, sex, and ancestry proportion/admixture; *q* value, FDR-corrected *P* value.

significant in BMI-corrected eQTL analysis (FDR <4% [in Supplementary Table 4*C*]), and results from both analysis (β and $-\log_{10}$ *P* value) were highly correlated ($r^2 > 0.9$). Thus, adipose tissue expression levels of these 587 transcripts are correlated with insulin sensitivity and are genetically regulated in both ethnicities. These transcripts were ranked based on their statistical significance of correlation with Matsuda index and association with genotype in eQTL analysis in AAGMEx and METSIM cohorts. The top 10 Matsuda index–correlated *cis*-eGenes are shown in Table 2. Based on average ranking, the enoyl-CoA hydratase domain-containing 3 (*ECHDC3*) gene was the top-ranked Matsuda index–correlated *cis*-eGene. Its expression was positively correlated with Matsuda index (ILMN_2072178, β = 1.009, $P = 6.29 \times 10^{-15}$ in AAGMEx [Fig. 1*A*] and 11728810_a_at, β = 0.34, $P = 2.35 \times 10^{-22}$, in METSIM [Supplementary Fig. 2*B*]). Adipose tissue *ECHDC3* expression was strongly regulated by *cis*-eQTL ($P = 1.94 \times 10^{-9}$ in AAGMEx and $P = 8.26 \times 10^{-52}$ in METSIM [Fig. 1*B* and Supplementary Fig. 2*C* and *D*]).

Ten genotyped SNPs (within ±500 Kb of transcript and MAF >0.01) showed significant association ($q < 0.04$) with *ECHDC3* transcript levels in adipose tissue of African Americans in the AAGMEx cohort, with rs200943982_T being the strongest genotyped *cis*-eSNP (MAF 0.393, β = −0.281, $P = 1.94 \times 10^{-9}$ [Fig. 1*B*]). Expanded eQTL analysis using imputed SNPs identified 53 *cis*-eSNPs ($P < 1 \times 10^{-4}$) in AAGMEx; rs34844369_A, an imputed SNP, was the strongest *cis*-eSNP (MAF 0.438, β = −0.283, $P = 9.37 \times 10^{-10}$ [Fig. 1*C*]) for *ECHDC3* (Supplementary Table 5). *ECHDC3* expression was positively correlated with Matsuda index in all genotype groups (Supplementary Fig. 4). The rs34844369 SNP is located in the intron of *ECHDC3* and rs200943982 is located downstream (~6.2 Kb 3′ of *ECHDC3*). These two *cis*-SNPs are 7,717 bp apart on chromosome 10 but showed moderate linkage disequilibrium (D′ = 0.89, $r^2 = 0.67$). Neither SNP was significantly associated with *ECHDC3* expression with adjustment for the other. Stepwise regression analysis identified no other significant eSNPs after adjustment for rs200943982 and rs34844369. Haplotype analyses of rs34844369 and rs200943982 suggested significant associations with *ECHDC3* expression level (global haplotype test $P = 1.32 \times 10^{-13}$), with the A-T haplotype (rs34844369_A-rs200943982_T) associated with reduced *ECHDC3* expression (β = −0.2976, $P = 2.75 \times 10^{-15}$, adjusted for age, sex, admixture). In the METSIM cohort, rs34844369 was a significant *ECHDC3* *cis*-eSNP ($P = 1.41 \times 10^{-32}$ [Supplementary Table 6]). However, in METSIM, the strongest *ECHDC3* *cis*-eQTL signal was identified at SNP rs3814627_G (MAF 0.312, β = −0.755, $P = 8.26 \times 10^{-52}$ [Supplementary Fig. 1*D*]), located in the putative *ECHDC3* promoter region (−482 bp upstream of the transcription start site). The SNP rs3814627 was not a significant *cis*-eSNP in AAGMEx (MAF 0.122, *P* = 0.68); however, another SNP near this putative promoter region (rs10906007_G, $P = 8.44 \times 10–7$, −1,157 bp upstream of the transcription start site) was significantly associated, suggesting the presence of common and ethnicity-specific genetic regulation for *ECHDC3* expression in adipose tissue. Epigenetic regulatory annotation of SNPs in *ECHDC3* *cis*-eQTL identified in the AAGMEx and METSIM cohorts, and the GTEx study by HaploReg v4.1 (https://pubs.broadinstitute.org/mammals/haploreg/haploreg.php), suggested the presence of promoter or enhancer histone marks and altered transcription factor–binding motifs for many of these *cis*-eSNPs (Supplementary Table 7*A*). Bioinformatic analysis using RegulomeDb-v1.1 (http://regulomedb.org/) and SNP2TFBS (https://ccg.vital-it.ch/snp2tfbs/) also supported the putative regulatory role and ability to alter transcription factor binding of these SNPs in *ECHDC3* *cis*-eQTL (Supplementary Table *B* and *C*). Despite a strong effect of regulatory genetic variants on proximal molecular phenotypes, i.e., transcript expression, these *cis*-eSNPs individually showed no statistically significant association with Matsuda index in either the AAGMEx or the METSIM cohort (Supplementary Tables 5 and 6). However, large genome-wide association study data sets curated in the Accelerating Medicines Partnership Type 2 Diabetes Knowledge Portal (http://www.type2diabetesgenetics.org/) for glycemic traits showed significant association (below genome-wide threshold) of top *ECHDC3* *cis*-eSNPs, and allele effect direction on traits was consistent with their effect on gene expression in our eQTL analysis. For example, rs3814627_G allele that reduces *ECHDC3* expression was associated with reduced Stumvoll insulin sensitivity index (β = −0.023, *P* = 0.0448) and increased HbA_{1c} (β = 0.027, *P* = 0.0309) in MAGIC (Meta-Analyses of Glucose and Insulin-related traits Consortium) genome-wide association study data sets.

ECHDC3 Is Primarily Expressed in Adipocytes

Human cohort analyses suggested that genetically regulated expression of *ECHDC3* in adipose tissue may be important in determining insulin sensitivity. Defining the contribution of adipose tissue cell types in *ECHDC3* expression levels may help identify cell-specific roles in correlations between *ECHDC3* expression and the Matsuda index. Thus, we fractionated fresh subcutaneous adipose tissue into adipocytes and adipose stromal vascular cells as previously described (28). Total RNA extracted from five to six African American individuals in the AAGMEx cohort was used to prepare separate pools of adipocyte fraction and stromal vascular fraction cDNA. In a qRT-PCR assay, *ECHDC3* expression was 13.6-fold higher in the adipocyte fraction (relative expression mean ± SD 11.53 ± 0.04) than the stromal vascular fraction (relative expression 0.85 ± 0.22) (Fig. 2*A*), suggesting that *ECHDC3* expression is primarily attributable to adipocytes.

Adipocyte Differentiation Induces *ECHDC3* Expression

We analyzed the expression of *ECHDC3* transcripts at different stages of in vitro differentiation of hADSCs

Table 2—Top 10 ranked Matsuda insulin sensitivity–correlated *cis*-eGenes in adipose tissue from African American (AAGMEx cohort) and European ancestry (METSIM) individuals

		AAGMEx cohort								METSIM cohort							
		Matsuda insulin sensitivity index			eQTL analysis					Matsuda insulin sensitivity index			eQTL analysis				
Gene symbol	Chr	ρ	*P*	Probe ID	Top *cis*-eSNP	A1	MAF	β*	eQTL_ *P* value	β	*P* value	Probeset ID	Top *cis*-eSNP	alt_ allele	MAF	β*	eQTL_ *P* value
ECHDC3	10	0.471	5.33E-15	ILMN_2072178	rs200943982	T	0.401	−0.281	1.94E-09	0.342	2.35E-22	11728810_a_at	rs3814627	G	0.312	−0.755	8.3E-52
MIF	22	−0.390	2.26E-10	ILMN_1807074	rs4822455	T	0.435	−0.188	4.56E-13	−0.257	5.64E-13	11744470_x_at	rs4822443	A	0.225	−0.989	1.3E-78
CENPV	17	0.411	1.86E-11	ILMN_3246608	rs3112521	T	0.427	0.107	5.83E-09	0.288	4.85E-16	11722721_a_at	rs3112526	C	0.485	0.751	2.3E-53
DDT	22	0.362	4.71E-09	ILMN_1690982	rs79966373	G	0.178	−0.302	2.81E-14	0.277	5.30E-15	11731089_a_at	chr22:24334948	C	0.353	−1.055	1E-125
APOB	2	0.401	6.50E-11	ILMN_1664024	rs1429974	T	0.241	0.293	5.28E-09	0.256	7.13E-13	11758033_s_at	rs11693870	C	0.265	0.950	9E-72
ORMDL3	17	0.445	2.24E-13	ILMN_1662174	rs28820390	A	0.091	−0.355	3.37E-07	0.392	1.52E-29	11736188_a_at	rs2872516	T	0.495	−0.565	1.2E-29
GLIPR1	12	−0.458	3.55E-14	ILMN_1769245	rs117251563	A	0.013	0.705	8.07E-07	−0.217	1.30E-09	11721839_at	rs35619460	C	0.194	−1.445	1E-158
ACSS3	12	0.449	1.32E-13	ILMN_1659885	rs4842386	G	0.167	−0.111	6.97E-06	0.332	2.99E-21	11759049_at	rs3794325	A	0.332	−0.919	5.9E-81
ITIH5	10	−0.434	9.54E-13	ILMN_1731862	rs201694044	G	0.375	−0.154	5.05E-07	−0.325	2.66E-20	11734677_x_at	rs867490	G	0.312	0.610	6.8E-33
DMRT2	9	0.401	6.05E-11	ILMN_1751785	rs756145	G	0.315	0.282	2.77E-08	0.300	1.80E-17	11727728_a_at	rs10959032	T	0.271	−0.699	9.4E-37

Matsuda insulin sensitivity–correlated transcripts of Entrez ID genes in adipose tissue associated with a SNP (q value <0.04) within $\pm$500 Kb of the 5′ and 3′ end of the transcript in AAGMEx are shown. Data for most significantly associated genotyped *cis*-eSNP in AAGMEx are presented. Data on European ancestry males are from the METSIM cohort (Civelek et al. [20]). In AAGMEx: ρ, Spearman partial correlation coefficient; *P* value, significance level of correlation of transcript level with Matsuda index in Spearman partial correlation analysis; A1, minor allele; β, effect size of minor allele (A1); eQTL_*P* value, significance in additive model (in MatrixEQTL analysis). In METSIM: β, β value; *P* value, significance level of correlation of transcript level with Matsuda index in linear regression analysis; alt_allele, alternative allele; β*, effect size for alternative allele of best *cis*-eSNP in FaST-LMM eQTL analysis. Results for all significant probes are shown in Supplementary Table 4. Top *cis*-eSNPs are not the same in both cohorts, but comparison of their effects is shown in Supplementary Table 4*A* and *B* and in Supplementary Fig. 3. Chr, chromosome.

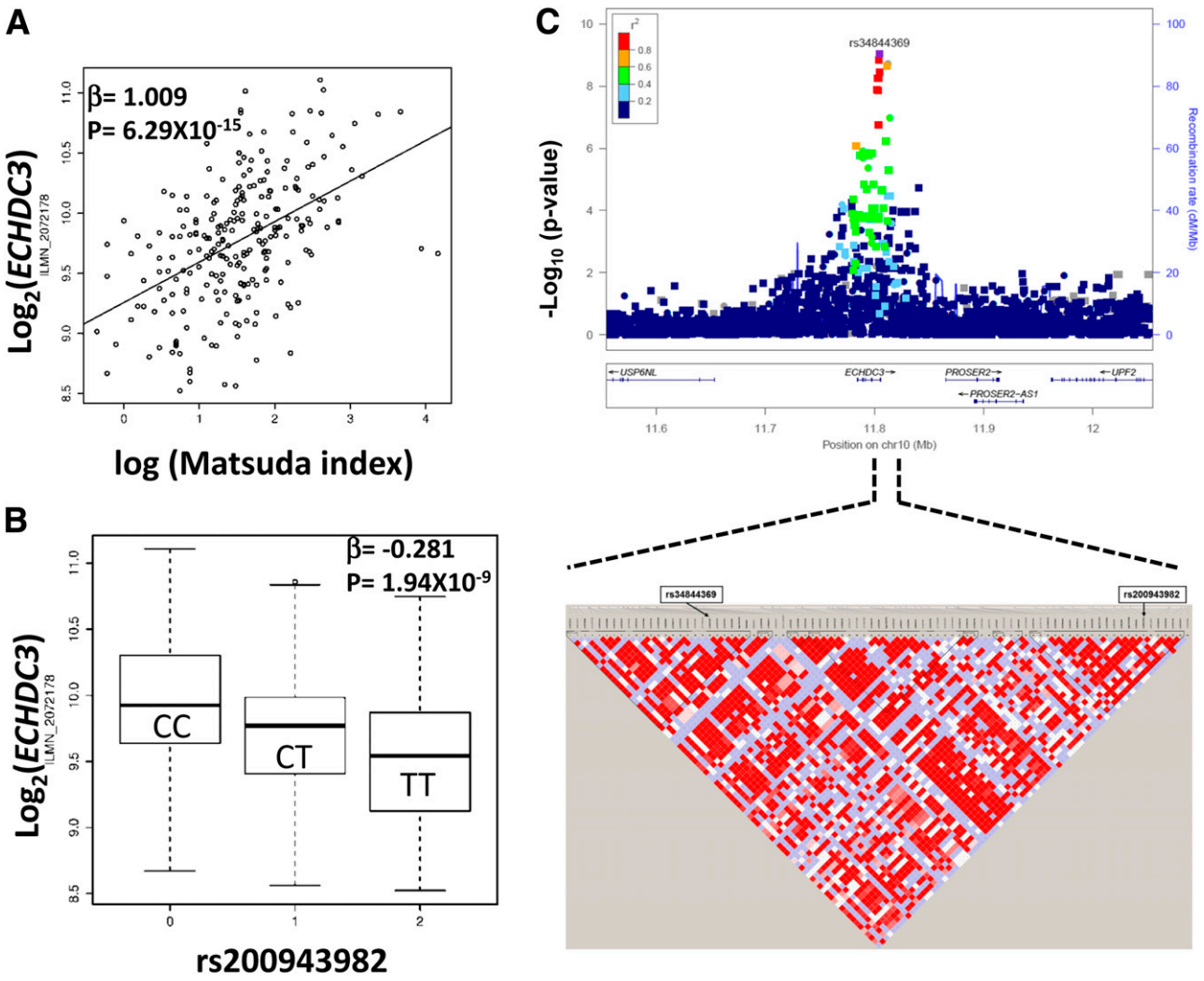

Figure 1—*ECHDC3* transcript expression in adipose tissue is correlated with Matsuda index of insulin sensitivity and is genetically regulated in African Americans. The scatter plot shows correlation of *ECHDC3* transcript expression (ILMN_2072178) in adipose tissue with Matsuda index in AAGMEx (*A*). The box plot shows association of *ECHDC3* transcript expression (ILMN_2072178) in adipose tissue with genotype of the *cis*-eSNP rs200943982 (*B*). LocusZoom plots show regional association of *ECHDC3 cis*-eQTL region SNPs (genotyped and imputed) with transcript expression (*C*). Significance level ($-\log_{10} P$ values) of genotyped SNPs are indicated as circles and imputed SNPs are indicated as squares in the LocusZoom plot. Linkage disequilibrium plot below the LocusZoom plot shows linkage disequilibrium relationship (r^2) between SNPs in the marked region and indicates the location of top imputed and genotyped *cis*-eSNP for *ECHDC3*, rs34844369 and rs200943982, respectively.

and SGBS cells. *ECHDC3* mRNA expression was low in undifferentiated hADSCs (relative expression 0.05 ± 0.01), began to rise in cells after 7 days in differentiation media, and was strongly induced at 14 days (relative expression 1.01 ± 0.02) (Fig. 2*B*). Similarly, *ECHDC3* mRNA expression at 14 days was 23-fold higher in SGBS cells compared with undifferentiated cells (Fig. 2*C*).

ECHDC3 Silencing in SGBS Adipocytes Decreases Insulin Sensitivity

Individuals with low mRNA abundance of *ECHDC3* in adipose tissue had low insulin sensitivity. Thus, we next determined whether decreasing *ECHDC3* expression in cultured human adipocytes reduced insulin sensitivity. SGBS cells stably expressing *ECHDC3*-specific shRNA (ECHDC3-KD) showed 70% downregulation ($P = 1.20 \times 10^{-5}$) of *ECHDC3* mRNA (Fig. 3*A*) compared with cells stably expressing control shRNA at 14 days after the induction of differentiation. Insulin (1 μmol/L) stimulated glucose uptake by 84% in control cells ($P = 0.009$) relative to PBS controls, but only 32% in ECHDC3-KD cells, demonstrating that insulin-stimulated glucose uptake was significantly ($P = 0.03$) decreased in *ECHDC3*-shRNA SGBS cells (ECHDC3-KD) compared with controls (Fig. 3*B*). As shown in a representative Western blot in Fig. 3*C*, pAkt at Ser^{473} after insulin stimulation was significantly decreased ($P = 0.0004$) (Fig. 3*D*) in ECHDC3-KD cells compared with controls.

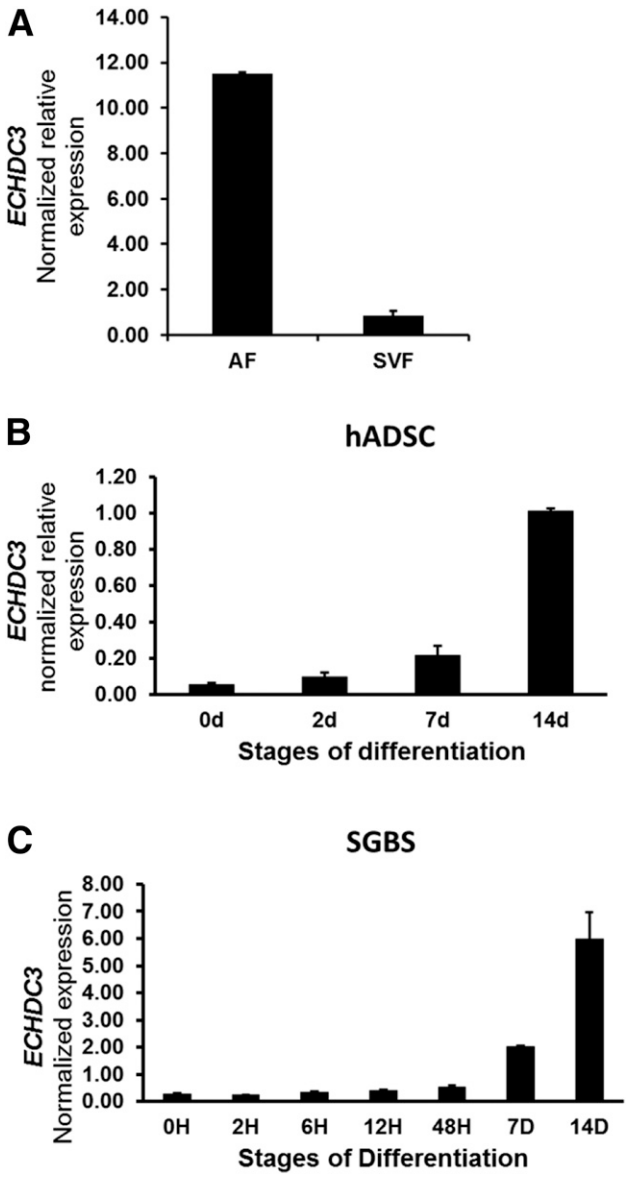

Figure 2—In subcutaneous adipose tissue, *ECHDC3* is primarily expressed in adipocytes and *ECHDC3* expression is induced with adipocyte differentiation. Results from the qRT-PCR analysis of expression of *ECHDC3* mRNA (normalized to *RPLP0* [36B4] endogenous control gene) are shown. *A*: Relative expression of *ECHDC3* in pooled RNA samples from stromal vascular fractions (SVFs) compared with the adipocyte fraction (AF) of subcutaneous adipose tissue in African Americans (data for two technical replicates of the pooled RNA samples from 5–6 individual donors are shown). Expression of *ECHDC3* at different stages of in vitro differentiation of hADSCs (*B*) and SGBS preadipocytes (*C*). Data are shown for independent biological triplicates at each stage of differentiation. d and D, days; H, hours.

ECHDC3 Silencing in Adipocytes Modulates Many Pathways and Genes Correlated With IR and Metabolism of Fatty Acid and Triacylglycerol

The functional role of *ECHDC3* in adipocytes or other cells is unknown. Our qRT-PCR analyses suggested significant downregulation of three genes important in IR—adiponectin (*ADIPOQ*) ($P = 1.15 \times 10^{-3}$), facilitated glucose transporter-4 (GLUT4/*SLC2A4*) ($P = 3.36 \times 10^{-6}$), and peroxisome proliferator–activated receptor γ (*PPARG*) ($P = 2.51 \times 10^{-6}$)—in *ECHDC3*-shRNA SGBS cells (ECHDC3-KD) compared with controls (Fig. 4*A*). To identify genes modulated by *ECHDC3* and to define its biological role, we compared triplicate cultures of *ECHDC3*-shRNA SGBS cells (ECHDC3-KD) with control-shRNA SGBS cells at day 14 of differentiation by RNA-seq analysis. This genome-wide analysis identified 691 DEGs (at Bayes posterior probability >70% and average $\log_2$ fold change ±0.58) in ECHDC3-KD cells compared with control cells (Fig. 4*B* and Supplementary Table 8), including 479 downregulated and 212 upregulated genes. The IPA result suggested an enrichment of 63 canonical pathways ($P < 0.05$) among DEGs, with the γ-linolenate biosynthesis pathway as the most enriched ($P = 3.8 \times 10^{-8}$) (Supplementary Table 9). Eight genes in this pathway (e.g., *FADS1*, *FADS2*, *ACSL1*, *ACSL5*) were downregulated in ECHDC3-KD cells. Downregulation of *FADS1* ($P = 9.44 \times 10^{-5}$) in ECHDC3-KD cells was validated by qRT-PCR in independent experiments (Fig. 4*C*). Canonical pathways for fatty acid, triglycerides, and cholesterol biosynthesis were also enriched among DEGs. Among the enriched pathways, expression profile of genes suggested significant inactivation of an LXR/RXR activation pathway ($P = 2.04 \times 10^{-7}$, $z = -2.53$). The IPA results also suggested enrichment of disease or biological function, including metabolism of triacylglycerol (17 genes, $P = 4.54 \times 10^{-13}$), fatty acid metabolism (51 genes, $P = 1.54 \times 10^{-10}$), and IR (25 genes, $P = 1.63 \times 10^{-8}$) (Fig. 4*D* and Supplementary Table 10). Regulator effects analysis considered DEGs in ECHDC3-KD cells and suggested an effect of upstream regulators on the expression of downstream target molecules and impact on biological function and diseases. The top two regulatory networks with a consistency score >20 suggested derangement in the accumulation of lipid, adipogenesis, and fatty acid metabolism in ECHDC3-KD cells (Fig. 4*E* and Supplementary Table 11). Thus, *ECHDC3* knockdown in adipocytes may cause IR by deranging multiple key biological pathways.

DISCUSSION

Our results suggest that gene expression levels in adipose tissue are key trans-ethnic (trans-ancestral) biomarkers strongly correlated with modulation of insulin sensitivity. Expression levels of transcripts for thousands of protein-coding genes in adipose tissue correlated with the Matsuda index, a well-validated estimate of insulin sensitivity measured by physiologically relevant OGTT (29). Thus, IR involves activation and repression of multiple pathways. We found that expression levels of a subset of these IR-correlated transcripts in adipose tissue are regulated by DNA sequence variants. The identification of eQTL for IR-correlated transcripts in adipose tissue suggests that the expression of these transcripts is at least partially genetically driven and causal and not just the result of altered insulin sensitivity. Comparing two cohorts, one of

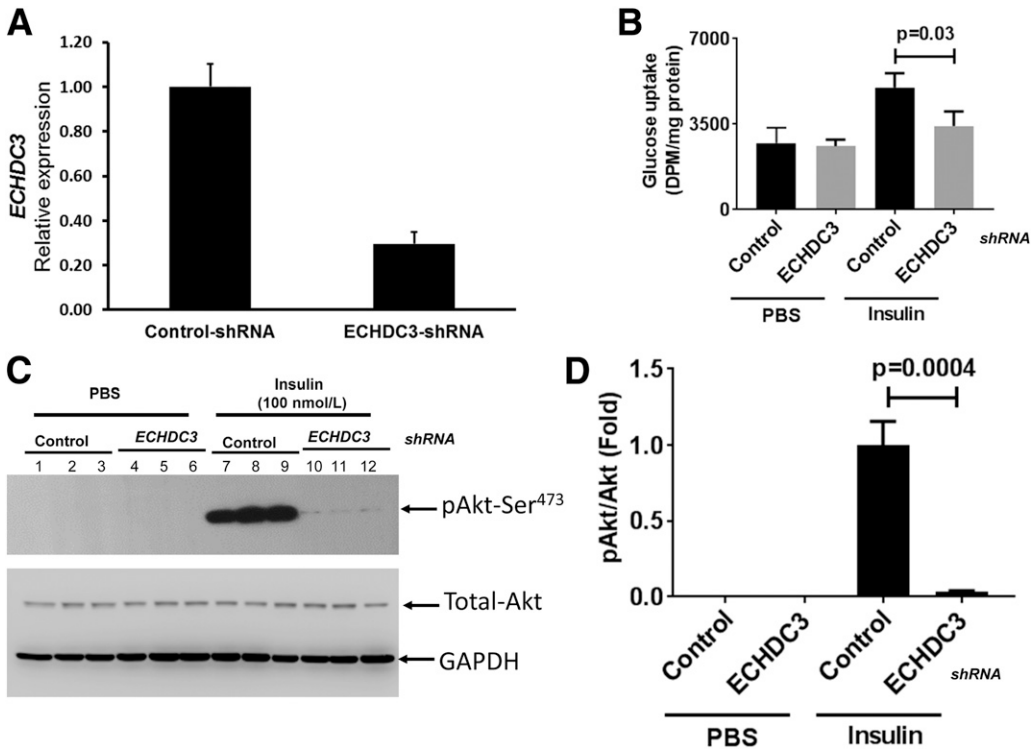

Figure 3—Knocking down of *ECHDC3* gene in SGBS adipocytes affects insulin sensitivity. *A*: Lentiviral particle-mediated delivery of gene-specific shRNA expression vector stably knocks down *ECHDC3* mRNA levels in SGBS adipocytes. Results from the qRT-PCR analysis of expression of *ECHDC3* mRNA (normalized to *RPLP0* [36B4] endogenous control gene) in SGBS cells stably expressing control shRNA or *ECHDC3* shRNA at 14 days post–initiation of differentiation are shown. Bar graph indicates the mean ± SD of six biological replicates for each condition from two independent experiments. *B*: Basal and insulin-stimulated glucose uptake in control shRNA and *ECHDC3* shRNA (ECHDC3-KD) SGBS cells at 14 days of differentiation. Bar graph indicates the mean ± SD of biological triplicates for each condition. Western blot analysis at day 14 of differentiated control shRNA and ECHDC3-KD SGBS cells using antibodies specific for pAKt, total Akt, and GAPDH at basal and insulin-stimulated (100 nmol/L for 15min) conditions (*C*) and quantified data (mean ± SD of biological triplicates) from scanning of a representative (selected from two independent experiments) Western blot (*D*) are shown. DPM, disintegrations per minute.

African Americans and one of European ancestry, provides independent validation and generalizability of our findings. The causal role of the *ECHDC3* gene in IR, a candidate gene identified through variation-based statistical genetic analyses, was validated through genetic silencing and functional studies in an adipocyte model.

In this study, we compared gene expression profiles from subcutaneous adipose tissues in an African American and a European ancestry cohort, primarily to identify trans-ancestral genetically regulated mechanisms of IR. We identified 3,755 genes with transcript levels significantly correlated with the Matsuda index and in the same direction of effect in both cohorts. These data support the concept of common molecular mechanisms of IR in both European and African ancestry. We further focused on these replicated insulin sensitivity–correlated genes and their regulation mediated by QTLs to define common causal mechanisms of IR. However, the genetic regulatory architecture of a subset of IR-correlated genes differs between ethnic groups, and comparison of ethnicities may be instrumental in identifying putatively ancestry-specific biological mechanisms of IR.

We identified 654 transcripts significantly correlated with the Matsuda index in our African American cohort (AAGMEx, FDR $P \leq 0.01$), but probes representing corresponding transcripts in the European ancestry cohort (METSIM) showed no significant correlation ($P > 0.05$); whether these transcript–Matsuda index correlations represent true African-derived mechanisms or false statistical correlations (i.e., type 1 errors) remains to be determined. As examples, expression of SFFV proviral integration oncogene-1 (*SPI1*) in adipose tissues of AAGMEx participants was significantly inversely correlated with Matsuda index (ILMN_1696463, NM_001080547, $\beta = -1.19$, $P = 2.97 \times 10^{-13}$; ILMN_2392043, NM_003120, $\beta = -1.13$, $P = 1.21 \times 10^{-11}$), but its expression was not significantly correlated in the METSIM cohort (represented by probe 11723165_a_at). The *SPI1* gene encodes for PU.1, a key transcription factor involved in monocyte-to-macrophage differentiation (30), and also plays a role in adipocyte inflammatory mechanisms causing IR (31,32). Despite the larger size of the METSIM cohort, this lack of replication may suggest that the effect of *SPI1* gene predominates in individuals of African ancestry. However, we also noted an

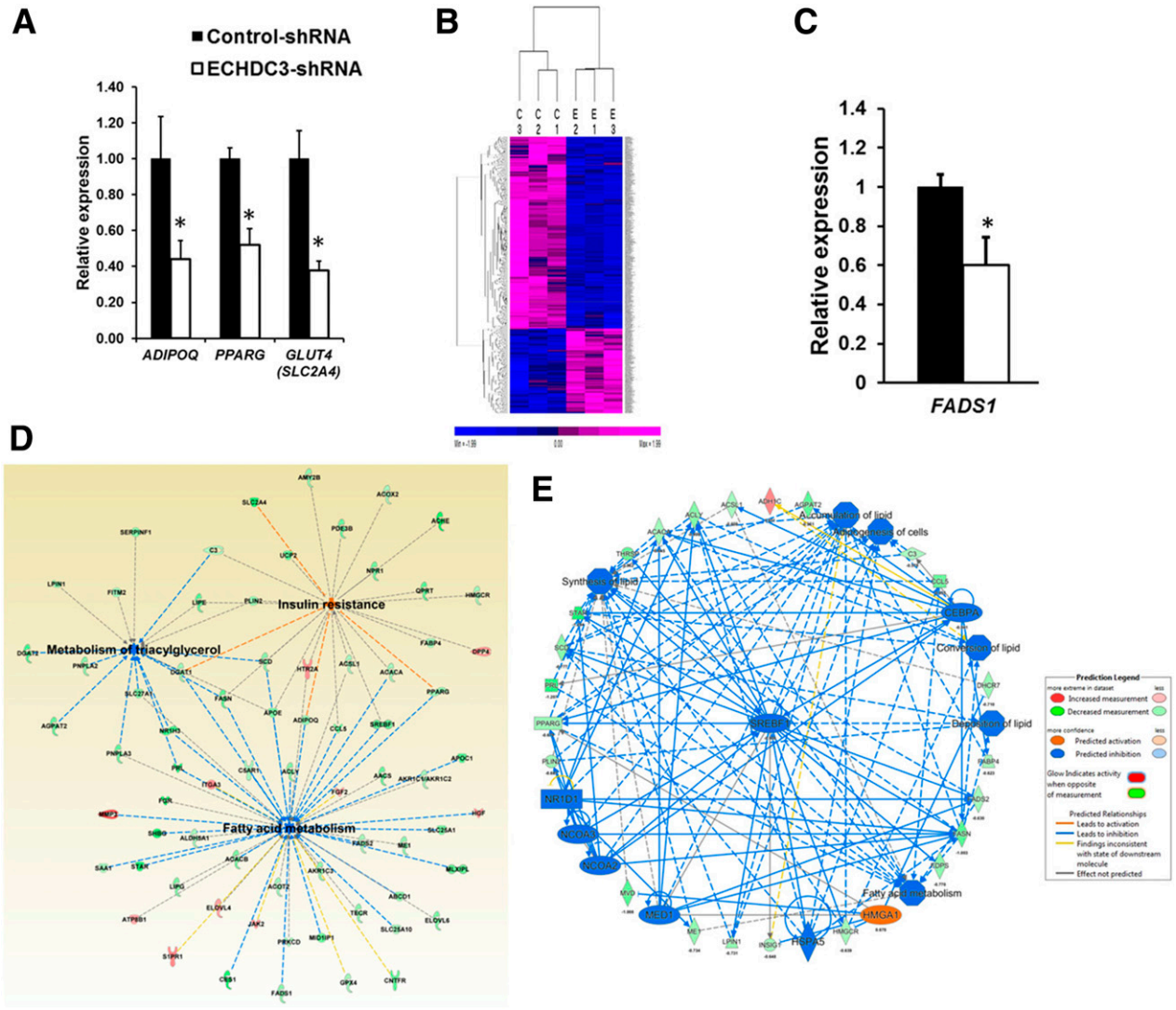

Figure 4—Knocking down *ECHDC3* gene in adipocytes modulates many pathways including genes in insulin sensitivity. *A*: Bar graph showing results from the qRT-PCR analysis of expression of adiponectin (*ADIPOQ*), peroxisome proliferator–activated receptor γ (*PPARG*), and facilitated glucose transporter-4 (GLUT4/*SLC2A4*) mRNA (normalized to *RPLP0*) in SGBS cells stably expressing control shRNA or *ECHDC3* shRNA at 14 days post–initiation of differentiation. Bar graph indicates the mean ± SD of six biological replicates for each condition from two independent experiments. $^*P < 0.01$. *B*: Heat map from unsupervised hierarchical clustering showing expression of 691 DEGs in ECHDC3-KD (*E*) compared with control shRNA–treated (*C*) SGBS cells at day 14 of differentiation. The expression levels of genes from RNA-seq analysis (FPKM values) were *z* score transformed for clustering analysis. The intensity of purple and blue color in heat map indicates the degree of high and low expression of transcripts, respectively. *C*: qRT-PCR analysis validates downregulation of fatty acid desaturase 1 (*FADS1*) in ECHDC3-KD SGBS cells in six biological replicates for each condition from two independent experiments. *D*: A network diagram from IPA that includes selected DEGs in ECHDC3-KD cells, significantly enriched for genes involved in the metabolism of triacylglycerol, fatty acid metabolism, and IR. *E*: Top regulatory network (consistency score = 20.85 and 37 nodes) identified by regulator effects analysis in IPA connected 23 DEGs with eight putative network regulators in ECHDC3-KD cells and suggested its impact on multiple biological processes in adipocytes including accumulation of lipid and adipogenesis.

inverse correlation between *SPI1* expression in adipose tissue and insulin sensitivity (Spearman semipartial $\rho = -0.40$, $P < 0.0001$ for ILMN_1696463) in another small cohort ($N = 99$) of European American individuals recruited from Arkansas in a previously published study (33). Gene expression data in the METSIM cohort were generated using the Affymetrix U219 array, while Illumina HumanHT-12 v4 Expression BeadChips were used for the AAGMEx cohort. Probes may have quantified different transcript isoforms or may have different efficiencies in the quantification of this gene. Thus, lack of replication, at least for a subset of these genes, may reflect technical rather than true biological difference between ethnicities and may be explained by such differences in probes. Our future studies will use alternative strategies that focus on ancestry-specific or ethnically predominant mechanisms of IR.

This study identified *cis*-eQTL for 587 Matsuda index–correlated transcripts in both the AAGMEx and METSIM

cohorts. Thus, in line with the anticipated polygenic nature of the insulin sensitivity phenotype, genetic regulation of a large subset of genes in adipose tissue may, at least in part, be causally involved in the pathogenesis of IR in African and European ancestry populations. These IR-correlated *cis*-eGenes are enriched for cellular functions and biological pathways. However, the precise role of many of these genes in IR is not known. To prioritize and begin to understand the role of genes in modulating cellular and molecular mechanisms causing IR, we ranked this large list of transcripts based on their statistical significance of correlation with the Matsuda index and association with genotype. *ECHDC3*, macrophage migration inhibitory factor (*MIF*), centromere protein V (*CENPV*), D-dopachrome tautomerase (*DDT*), and apolipoprotein B (*APOB*) were among the top Matsuda index–correlated *cis*-eGenes. Some of these genes have a known role in adipose tissue biology and IR. For example, macrophage migration inhibitory factor superfamily gene members *MIF* and *DDT* bind to the CD74/CD44 receptor complex and have distinct roles in adipogenesis. *MIF* positively correlates with IR and contributes to adipose tissue inflammation by modulating adipose tissue macrophage functions, while *DDT* reverses glucose intolerance (34,35).

The *ECHDC3* gene emerged as the most significant Matsuda index–correlated *cis*-eGene. Multitissue expression data from the GTEx study showed high *ECHDC3* expression in fatty acid metabolizing tissues, including liver, muscle, and adipose. Strong *cis*-eQTL associations were detected for ECHDC3 expression in subcutaneous adipose tissue in GTEx V7-P2 (rs10906007, $P = 1.40 \times 10^{-10}$ [https://gtexportal.org/]) and STARNET (Stockholm-Tartu Atherosclerosis Reverse Networks Engineering Task) (36) (rs718641, $P = 4.78 \times 10^{-10}$) studies. However, its role in adipose or other tissue is unknown. Based on protein sequence homology, peroxisomal enoyl-CoA hydratase (*ECH1*) and short-chain acyl-CoA dehydrogenase (*ECHS1*/SCHE) are the closest human homologs. This suggests that *ECHDC3* may act as enoyl-CoA hydratase. The enoyl-CoA hydratase is a key mitochondrial enzyme involved in fatty acid β-oxidation and catalyzes the addition of H_2O across the double bond of *trans*-2-enoyl-CoA, resulting in formation of a β-hydroxyacyl-CoA (37). Biochemical analyses suggest that human *ECHDC1*, a likely homolog of *ECHDC3*, lacks enoyl-CoA hydratase activity (38). A recent study suggested that *ECHS1*, a close homolog of *ECHDC3*, senses nutrient signals and acts as the converging enzyme for fatty acid and branched-chain amino acid oxidation (39).

Supporting a connection between decreased *ECHDC3* expression in adipose tissue and IR, in vitro knockdown of *ECHDC3* expression in our study significantly downregulated insulin signaling and insulin-stimulated glucose uptake in human adipocytes. Our unbiased transcriptome-wide analysis suggested that downregulation of *ECHDC3* in human adipocytes may cause IR by significantly inactivating fatty acid biosynthesis, including the γ-linolenate biosynthesis, cholesterol biosynthesis, and LXR/RXR activation pathways. Genetic polymorphisms in the *ECHDC3* regulatory element (eQTL) determine a significant proportion of its variable expression in adipose tissue, likely by their differential ability to interact (as suggested by SNP2TFBS and RegulomeDb) with transcription factors. A regulatory element in the intron of *ECHDC3* (near SNP rs34844369) was observed in both European and African ancestry cohorts, while an additional regulatory element upstream to *ECHDC3* (−400 bp to −4 Kb, near SNP rs3814627) was observed only in European ancestry cohorts. These two regions are not in linkage disequilibrium in African ancestry cohorts ($D' = 0.21$, $r^2 = 0.007$, 1KGP Phase 3_V5 data from LDlink: https://ldlink.nci.nih.gov/), but are in strong linkage disequilibrium in European ancestry cohorts ($D' = 0.95$, $r^2 = 0.63$). Future studies will define the transcriptional regulatory mechanisms mediated by these regulatory elements and their interactions that may have ancestry-specific contributions in determining genetic regulatory networks important for the pathogenesis of IR.

In summary, genetic regulation of a large subset of genes in adipose tissue is causally involved in the pathogenesis of IR in African and European ancestry individuals. Our variation-based genomic analysis with concurrent analyses of glucose-homeostasis phenotypes, adipose tissue transcriptome, and in vitro genetic silencing studies identified several genetic regulatory mechanisms, including the novel role of the *ECHDC3* gene in causing IR putatively by modulating fatty acid metabolism and other key pathways in adipocytes.

Acknowledgments. The authors thank Drs. Jorge Calles-Escandon, Jamel Demons, Samantha Rogers, and Barry Freedman and the dedicated staff of the Clinical Research Unit at Wake Forest School of Medicine (WFSM) for support of the clinical studies and assistance with clinical data management for the AAGMEx cohort. The authors thank Lata Menon, Joyce Byers, Ethel Kouba, and Donna Davis for support in participant recruitment for the AAGMEx cohort. The authors thank the staff in the Genomics Core Laboratory at the Center for Genomics and Personalized Medicine Research for their extensive support in genotyping and gene expression analysis using the Illumina microarray platform for the AAGMEx cohort. The authors thank the METSIM study investigators for publicly sharing their data. The authors acknowledge the WFSM Center for Public Health Genomics for computational resources. The authors also acknowledge the editorial assistance of Karen Klein at the Wake Forest Clinical and Translational Science Institute.

Funding. This work was primarily supported by the National Institute of Diabetes and Digestive and Kidney Diseases (NIDDK), National Institutes of Health, research grants R01 DK090111 and R01 DK118243 to S.K.D. This work was also supported by the National Heart, Lung, and Blood Institute (NHLBI) grant R00 HL121172 and NIDDK grant R01 DK118287 to M.C. and NHLBI grant R01 HL119962 to J.S.P.

Duality of Interest. No potential conflicts of interest relevant to this article were reported.

Author Contributions. N.K.S. performed genomic and cell biological experiments, analyzed data, and reviewed and edited the manuscript. C.-C.C.K. performed cell biological experiments, analyzed data, and reviewed and edited the manuscript. M.C. analyzed METSIM cohort data and reviewed and edited the

manuscript. M.W. supplied a critical reagent (SGBS cells) for this study and reviewed and edited the manuscript. M.E.C. performed statistical genetic analysis and reviewed and edited the manuscript. C.D.L. supervised statistical genetic analysis, interpreted data, and reviewed and edited the manuscript. J.S.P. supervised cell biological studies, interpreted data, and reviewed and edited the manuscript. S.K.D. designed the study, analyzed and interpreted data, and wrote the manuscript. C.D.L. and S.K.D. are the guarantors of this work and, as such, had full access to all the data in the study and take responsibility for the integrity of the data and the accuracy of the data analysis.

Prior Presentation. Parts of this study were presented in abstract form at the 78th Scientific Sessions of the American Diabetes Association, Orlando, FL, 22–26 June 2018.

References

1. Czech MP. Insulin action and resistance in obesity and type 2 diabetes. Nat Med 2017;23:804–814
2. Tabák AG, Jokela M, Akbaraly TN, Brunner EJ, Kivimäki M, Witte DR. Trajectories of glycaemia, insulin sensitivity, and insulin secretion before diagnosis of type 2 diabetes: an analysis from the Whitehall II study. Lancet 2009;373:2215–2221
3. Mercado MM, McLenithan JC, Silver KD, Shuldiner AR. Genetics of insulin resistance. Curr Diab Rep 2002;2:83–95
4. Liu CT, Raghavan S, Maruthur N, et al.; AAAG Consortium; CARe Consortium; COGENT-BP Consortium; eMERGE Consortium; MEDIA Consortium; MAGIC Consortium. Trans-ethnic meta-analysis and functional annotation illuminates the genetic architecture of fasting glucose and insulin. Am J Hum Genet 2016;99:56–75
5. Manning AK, Hivert MF, Scott RA, et al.; DIAbetes Genetics Replication And Meta-analysis (DIAGRAM) Consortium; Multiple Tissue Human Expression Resource (MUTHER) Consortium. A genome-wide approach accounting for body mass index identifies genetic variants influencing fasting glycemic traits and insulin resistance. Nat Genet 2012;44:659–669
6. Saxena R, Hivert MF, Langenberg C, et al.; GIANT consortium; MAGIC investigators. Genetic variation in GIPR influences the glucose and insulin responses to an oral glucose challenge. Nat Genet 2010;42:142–148
7. Scott RA, Lagou V, Welch RP, et al.; DIAbetes Genetics Replication and Meta-analysis (DIAGRAM) Consortium. Large-scale association analyses identify new loci influencing glycemic traits and provide insight into the underlying biological pathways. Nat Genet 2012;44:991–1005
8. Knowles JW, Xie W, Zhang Z, et al.; RISC (Relationship between Insulin Sensitivity and Cardiovascular Disease) Consortium; EUGENE2 (European Network on Functional Genomics of Type 2 Diabetes) Study; GUARDIAN (Genetics UnderRlying DIAbetes in HispaNics) Consortium; SAPPHIRe (Stanford Asian and Pacific Program for Hypertension and Insulin Resistance) Study. Identification and validation of N-acetyltransferase 2 as an insulin sensitivity gene. J Clin Invest 2015;125:1739–1751
9. Palmer ND, Goodarzi MO, Langefeld CD, et al. Genetic variants associated with quantitative glucose homeostasis traits translate to type 2 diabetes in Mexican Americans: the GUARDIAN (Genetics Underlying Diabetes in Hispanics) Consortium. Diabetes 2015;64:1853–1866
10. Walford GA, Gustafsson S, Rybin D, et al. Genome-wide association study of the modified Stumvoll insulin sensitivity index identifies BCL2 and FAM19A2 as novel insulin sensitivity loci. Diabetes 2016;65:3200–3211
11. Gamazon ER, Segrè AV, van de Bunt M, et al.; GTEx Consortium. Using an atlas of gene regulation across 44 human tissues to inform complex disease- and trait-associated variation. Nat Genet 2018;50:956–967
12. Cannon ME, Mohlke KL. Deciphering the emerging complexities of molecular mechanisms at GWAS loci. Am J Hum Genet 2018;103:637–653
13. Rosen ED, Spiegelman BM. Adipocytes as regulators of energy balance and glucose homeostasis. Nature 2006;444:847–853
14. Badoud F, Perreault M, Zulyniak MA, Mutch DM. Molecular insights into the role of white adipose tissue in metabolically unhealthy normal weight and metabolically healthy obese individuals. FASEB J 2015;29:748–758
15. Samuel VT, Shulman GI. The pathogenesis of insulin resistance: integrating signaling pathways and substrate flux. J Clin Invest 2016;126:12–22
16. Elbein SC, Kern PA, Rasouli N, Yao-Borengasser A, Sharma NK, Das SK. Global gene expression profiles of subcutaneous adipose and muscle from glucose-tolerant, insulin-sensitive, and insulin-resistant individuals matched for BMI. Diabetes 2011;60:1019–1029
17. Emilsson V, Thorleifsson G, Zhang B, et al. Genetics of gene expression and its effect on disease. Nature 2008;452:423–428
18. Sharma NK, Sajuthi SP, Chou JW, et al. Tissue-specific and genetic regulation of insulin sensitivity-associated transcripts in African Americans. J Clin Endocrinol Metab 2016;101:1455–1468
19. Sajuthi SP, Sharma NK, Chou JW, et al. Mapping adipose and muscle tissue expression quantitative trait loci in African Americans to identify genes for type 2 diabetes and obesity. Hum Genet 2016;135:869–880
20. Civelek M, Wu Y, Pan C, et al. Genetic regulation of adipose gene expression and cardio-metabolic traits. Am J Hum Genet 2017;100:428–443
21. Wabitsch M, Brenner RE, Melzner I, et al. Characterization of a human preadipocyte cell strain with high capacity for adipose differentiation. Int J Obes Relat Metab Disord 2001;25:8–15
22. Vaittinen M, Kaminska D, Käkelä P, et al. Downregulation of CPPED1 expression improves glucose metabolism in vitro in adipocytes. Diabetes 2013;62:3747–3750
23. McGillicuddy FC, Chiquoine EH, Hinkle CC, et al. Interferon gamma attenuates insulin signaling, lipid storage, and differentiation in human adipocytes via activation of the JAK/STAT pathway. J Biol Chem 2009;284:31936–31944
24. Kim D, Langmead B, Salzberg SL. HISAT: a fast spliced aligner with low memory requirements. Nat Methods 2015;12:357–360
25. Langmead B, Trapnell C, Pop M, Salzberg SL. Ultrafast and memory-efficient alignment of short DNA sequences to the human genome. Genome Biol 2009;10:R25–R10
26. Li B, Dewey CN. RSEM: accurate transcript quantification from RNA-Seq data with or without a reference genome. BMC Bioinformatics 2011;12:323
27. Tarazona S, Furió-Tarí P, Turrà D, et al. Data quality aware analysis of differential expression in RNA-seq with NOISeq R/Bioc package. Nucleic Acids Res 2015;43:e140
28. Rodbell M. Metabolism of isolated fat cells. I. Effects of hormones on glucose metabolism and lipolysis. J Biol Chem 1964;239:375–380
29. Matsuda M, DeFronzo RA. Insulin sensitivity indices obtained from oral glucose tolerance testing: comparison with the euglycemic insulin clamp. Diabetes Care 1999;22:1462–1470
30. Gosselin D, Link VM, Romanoski CE, et al. Environment drives selection and function of enhancers controlling tissue-specific macrophage identities. Cell 2014;159:1327–1340
31. Lin L, Pang W, Chen K, et al. Adipocyte expression of PU.1 transcription factor causes insulin resistance through upregulation of inflammatory cytokine gene expression and ROS production. Am J Physiol Endocrinol Metab 2012;302:E1550–E1559
32. Lefterova MI, Steger DJ, Zhuo D, et al. Cell-specific determinants of peroxisome proliferator-activated receptor gamma function in adipocytes and macrophages. Mol Cell Biol 2010;30:2078–2089
33. Das SK, Sharma NK, Hasstedt SJ, et al. An integrative genomics approach identifies activation of thioredoxin/thioredoxin reductase-1-mediated oxidative stress defense pathway and inhibition of angiogenesis in obese nondiabetic human subjects. J Clin Endocrinol Metab 2011;96:E1308–E1313
34. Kleemann R, Bucala R. Macrophage migration inhibitory factor: critical role in obesity, insulin resistance, and associated comorbidities. Mediators Inflamm 2010;2010:610479
35. Kim BS, Pallua N, Bernhagen J, Bucala R. The macrophage migration inhibitory factor protein superfamily in obesity and wound repair. Exp Mol Med 2015;47:e161

36. Franzén O, Ermel R, Cohain A, et al. Cardiometabolic risk loci share downstream cis- and trans-gene regulation across tissues and diseases. Science 2016;353:827–830
37. Agnihotri G, Liu HW. Enoyl-CoA hydratase. Reaction, mechanism, and inhibition. Bioorg Med Chem 2003;11:9–20
38. Linster CL, Noël G, Stroobant V, et al. Ethylmalonyl-CoA decarboxylase, a new enzyme involved in metabolite proofreading. J Biol Chem 2011;286: 42992–43003
39. Zhang YK, Qu YY, Lin Y, et al. Enoyl-CoA hydratase-1 regulates mTOR signaling and apoptosis by sensing nutrients. Nat Commun 2017;8:464–00489